Nigerian Journal of Physics (NJP)
ISSN online: 3027-0936
ISSN print: 1595-0611
DOI: https://doi.org/10.62292/njp.v34i1.2025.386
Volume 34(1), March 2025

Induced Nonlinear Stretching Sheet Near a Stagnation Point for Nonlinear Mixed Convection in Williamson Nanofluid Flow

[*1]Hammed, F. A., [2]Akanbi, O. O., [1]Usman, M. A., [1]Onitilo, S. A., and [1]Adeyemi, I.

[1]Department of Mathematical Sciences, Olabisi Onabanjo University, Ago-Iwoye, Nigeria
[2]Department of Mathematics and Statistics, Federal Polytechnic, Ilaro, Nigeria

[*]Corresponding author's email: hammed.fatai@oouagoiwoye.edu.ng

ABSTRACT
The analysis of non-Newtonian nanofluid flows near stagnation points has become increasingly important due to its broad engineering and industrial applications, including polymer extrusion, biomedical engineering, and cooling of electronic devices. The Williamson fluid model, as a subclass of non-Newtonian fluids, captures shear-thinning behavior and provides a more accurate representation of complex fluids. This paper presents an investigation into the flow of a magnetized non-Newtonian Williamson fluid by nonlinear mixed convection. A stagnation point regulates the motion of the fluid. The Mathematical model underlying the problem is transmuted via similarity transformations to exhibit ordinary differential equations of order three. A numerical solution is obtained through the Runge-Kutta-Fehlberg approach in conjunction with the shooting technique. The influence of some dimensionless physical parameters which includes magnetic field, Eckert, Schmidt and Prandtl numbers coupled with activation energy were discussed through plots. The numerical results demonstrate a good agreement when compared with existing results. The analysis reveals a decrease in velocity profile and a rise in fluid temperature. This is observed when the magnitude of the viscosity and magnetic field parameters increases. An increase in radiation and heat source parameters leads to an increase in the heat transfer rate. Whereas those factors involving viscosity and magnetic field slow down the fluids and drive a rise in the temperature distribution. The solutal boundary structure is enhanced due to the escalating nature of activation energy. A diminished trend observed to occur with the chemical reaction and Schmidt number.

Keywords:
Dimensionless parameters,
Elongating sheet,
Nonlinear mixed convection,
Stagnation-point,
Williamson nanoliquid.

INTRODUCTION

The non-Newtonian fluids have been found to have numerous uses in a wide range of human undertakings. As a result, their studies are gaining much attention from various authors. This class of fluid is common in the oil drilling industry, paints rheology, molten polymers, mud drilling, the drug and pharmaceutical industry, the cosmetics industry. Several authors have reported on the importance of non-linear viscous fluids in industrial and engineering works (Fatumbi et al., 2020; Yusuf et al., 2021; Wang, 1984). Highly nonlinear and complex equations are required to describe the flow of non-linear viscous fluids, which differ significantly from the flow of linear viscous fluids due to the stress tensors' nonlinear relation to the deformation rate. Since no single constitutive model can fully account for the properties of these fluids, various theories and concepts have been developed to capture their flow characteristics. Some of the many fluid models used to describe non-Newtonian fluids are the Williamson fluid, the Carreau fluid, the Jeffery fluid, the Maxwell fluid, the micropolar fluid, and the Giesekus fluid (Nabwey and Mahdy, 2021; Pal and Chaterjee, n.d.; Sajjan et al., 2022).

The Williamson fluid model stands out among others. For instance, as shear stress rates increase, the viscosity fluid thins, demonstrating its non-Newtonian fluid nature. Notable among these class of fluids includes plasma blood and emulsion sheets like those used in photography. The pioneer studies was conducted in (Nadeem et al., 2013; Mahanthesh et al., 2020) where boundary layer transport of such fluids along a stretched surface was developed having acknowledged Williamson

(Qasim et al., 2013). This has led to a plethora of studies that consider various aspects, such as the geometry of the flow, heating conditions at the energy field, etc. In the investigation of the Williamson fluid on Blasius flow near a stagnation point, (Shah et al., 2013) investigated the significance of heat transmission in the existence of thermal radiation over the permeable elongated device. (Mabood et al., 2021; Quran et al., 2023) investigated how Williamson fluid is affected by forced convection forces and uniform heat transmission at the boundary using a numerical procedure on a porous material medium. The results obtained that the Williamson fluid has the tendency to increase the shear stress and the velocity profiles.

Flowing fluids across extending plates are often encountered in diverse areas of industry and technology. Many potential applications are found in the production of polymers, the process of shaping plastic sheets, papermaking, cooling of metal sheets and so on (Chao et al., 1965; Ibrahim and Suneetha, 2015; Pandey and Kumar, 2016; Nadeem et al., 2013; Williamson, 1929; Mabood et al., 2015). Such investigation evolved from the study of (Crane, 1970) where a closed-form solution was proposed to analyse a time-independent two-dimensional problem for which the sheet have extended in a linear form. Other studies in (Mabood et al., 2015; Fatumbi et al., 2023) have proposes the possibility of applying a nonlinear elongating sheet which has been found to be more realistic in practical applications situations such as wire drawing

Fluids composed of nanoparticles of metal oxides among others called nanofluids have been discussed in (Gupta and Gupta,1977; Mishra et al., 2016). Studies have been conducted revealing an enhanced thermal conductivity when these new fluid category is used compared to traditional carrier fluids including water, oil, ethylene glycol among others. The cooling process is vital in high-energy equipment such as those found in numerous engineering and industrial process (power production and nuclear reactors). Due to its potential usefulness in various fields relevant to modern society, including medicine, transportation, and electronics, (Cortel, 2007; Waqas et al., 2016; Choi, 1995) have reported that nanofluid research has continuously gained much scholarly attention.

The current study seeks to investigate the influence of various parameters such as magnetic field Eckert number, Schmidt, Prandtl and activation energy on the flow behavior of a reactive magnetized Williamson nanofluid in the presence of nonlinear mixed convection, activation energy, thermal radiation, thermo-migration of small particles, Brownian mobility of the particles, and convective heating of the thermal boundary region. The thermal conductivity and an external heat source is known to cause a nonlinearly expanding plate to undergo the motion. The study has important implications for chemical and extrusion operations in engineering applications. A computational method is employed to discuss the parametric effects of crucial terms on the dimensionless velocity, temperature, and concentration profiles of the relevant governing equations.

Development of the Problem

Figure 1 illustrates a Williamson nanoliquid flowing across a two-dimensional extending material device in the neighbourhood of a stagnation point. It is assumed that the fluid motion is time-independent it is simply laminar and not turbulent, and it is not compressible as well. The extending plate causes the flow and that the device stretches in a nonlinear fashion with the surface velocity $u_w = bx^m$ at the wall and velocity $U_e = ax^m$ at the far field. A convective heating type is adhered to in the thermal region, but the ambient temperature relates to that of the fluid. The coordinates of the material device are described using (x, y) and their respective velocity components are (u, v). The radiative heat flux is simplified by Rosseland approximation. This is to note that there is an internal heat generation in the energy field while the nanoparticles concentration field consists of the chemical reaction in conjunction with the activation energy. The application of varying external magnetic field on the direction of flow given as

$B(x)\left(B(x) = Bx^{\frac{m}{2}-\frac{1}{2}}\right)$

is done on the material device but no account of the initiated magnetic field is considered. The thermophysical attributes of the fluid are functions of temperature.

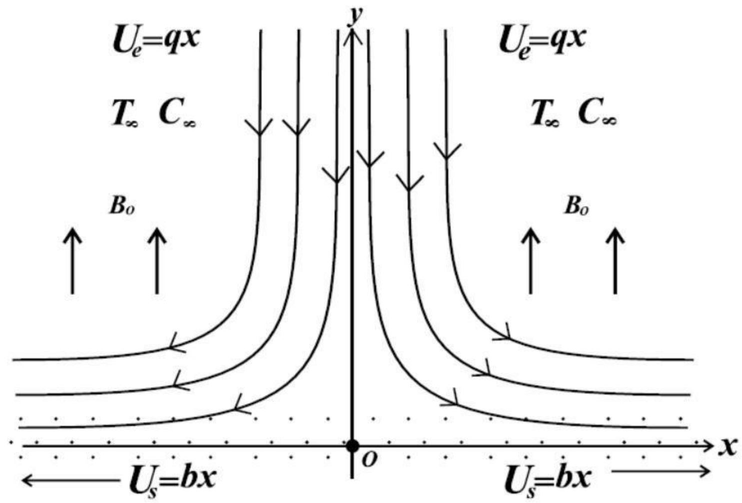

Figure 1: Sketch of the configuration

On the basis of the aforementioned assumptions, the transport equations are listed as follows:

$$\frac{\partial U}{\partial x}+\frac{\partial V}{\partial y}=0 \tag{1}$$

$$U\frac{\partial U}{\partial x}+V\frac{\partial V}{\partial y}-U_e\frac{dU_e}{dx}=\frac{\mu}{\rho_f}\frac{\partial^2 U}{\partial y^2}(1+\sqrt{2}\Gamma+g[\beta_1(T-T_\infty)+\beta_2(T-T_\infty)^2\,]+g(G-G_\infty)-\frac{\sigma}{\rho_f}\big(B(x)\big)^2(U-U_e) \tag{2}$$

$$U\frac{\partial U}{\partial x}+V\frac{\partial V}{\partial y}=\frac{\mu}{(\rho c_p)}\frac{\partial}{\partial y}\left(k\frac{\partial T}{\partial y}\right)+\gamma\left[\frac{D_T}{T_\infty}\left(\frac{\partial T}{\partial y}\right)^2+D_B\left(\frac{\partial T}{\partial y}\frac{\partial C}{\partial y}\right)\right]+\frac{Q(x)(T-T_\infty)}{(\rho c_p)_f}+\frac{\mu}{(\rho c_p)_f}\left[\left(\frac{\partial u}{\partial y}\right)^2+\Gamma\left(\frac{\partial U}{\partial y}\right)^3\right]+\frac{16\sigma^*}{3B_*(\rho c_p)_f}\frac{\partial}{\partial x}\left(T^3\frac{\partial T}{\partial y}\right)+\frac{\sigma}{(\rho c_p)_f}B\big((x)\big)^2(U-U_e)^2 \tag{3}$$

$$U\frac{\partial G}{\partial x}+v\frac{\partial G}{\partial y}=D_B\frac{\partial C^2}{\partial y^2}+\frac{D_T}{T_\infty}\left(\frac{\partial^2 T}{\partial y^2}\right)-k_1^2(G-G_\infty)\left(\frac{T}{T_\infty}\right)^a\exp\left(-\frac{E_e}{\lambda T}\right) \tag{4}$$

The corresponding boundary constraints are listed as:

$$U(x,y)=u=bx^m, V(x,0)=0.-k_\infty\frac{\partial T}{\partial y}=-g_b\big(T_\infty-T_f\big), G(x,y)=G_w\ at\ y=0 \tag{5}$$

$$u\to U_e=ax^m.T\to T_\infty.G\to G_\infty, as\ y\to\infty$$

Those symbols that are included in the governing equations are u,v which is a component of velocity in x,y directions, T indicating Temperature, v_∞ meaning ambient dynamic friction, G denoting nanoparticles concentration, ρ_∞which is ambient fluid density, U_e indicating far field velocity, μ_∞ meaning a ambient Fluid viscosity, U_w connoting surface velocity σ standing for electrical conductivity, h_T connoting coefficient of heat transfer, h_1 symbolizing chemical reaction rate, h_c is the mass transfer coefficient, Γ standing for the relaxation time, T_∞ indicating the far field temperature, (ρ_f) connoting nanofluid density, C_∞ indicating far field concentration. Similarly, (ρ_p) stands for nanoparticles density but E_0means activation energy while $(\rho c_p)_f$ indicates heat capacity of nanoparticles whereas $(\rho cp)_f$ shows the heat capacity of the fluid. More so, D_B represents coefficient of Brownian motion, D_T indicates thermophoretic diffusion coefficient, T_f is standing for surface temperature, G_w is symbolizing sheet concentration, and k stands for thermal conductivity.

Equations (7-9) are the result of plugging in the quantities from Eq. (6) in order to change the governing equations to their ordinary derivatives of order three. Using (6) also satisfies the equation of mass conservation (1).

$$\eta=y\left(\frac{bx^{r-1}}{v_\infty}\right)^{\frac{1}{2}},\psi=(v_\infty bx^{m+1})^{\frac{1}{2}}f(\eta),\phi(\eta)=\frac{G-G_\infty}{G_w-G_\infty},k=k_\infty(1+\alpha\theta) \tag{6}$$

$$(1+Wef'')f'''+ff''-\left(\frac{2m}{m+1}\right)f'^2+mK^2-\left(\frac{2m}{m+1}\right)M(f'-K)+\lambda_1\theta(1+\lambda_2\theta)+\lambda_3\phi=0 \tag{7}$$

$$(1+\alpha\theta+Nr)\theta''+\alpha\theta'^2+\left(\frac{m+1}{2}\right)Prf\theta'+PrEc\left(1+\frac{We}{\sqrt{2}}f''\right)f''^2+\mathrm{Pr}(N_t\theta'^2+N_b\theta'\phi')+PrQ\theta+PrEcM(f'-K)^2=0 \tag{8}$$

$$\phi''+\frac{N_t}{N_b}\theta''+\left(\frac{m+1}{2}\right)Scf\phi'-Sc\gamma_1(1+\beta\theta)^a\exp\left(-\frac{E}{1+\beta\theta}\right)\phi=0 \tag{9}$$

In the same vein, the wall constraints are transformed as follows

$$f'(\eta)=1,f(\eta)=0,0'(\eta)=-\zeta\big(1-\theta(0)\big),\phi(\eta)=1\ at\ \eta=0$$

$$f'(\eta)=H,\theta(\eta)=0,\phi(\eta)=0\ as\ \eta\to 0 \tag{10}$$

$Pr = \frac{\mu_\infty c_p}{k_\infty}, M = \frac{\sigma B_0^2}{b\rho}, Nr = \frac{16\sigma^* T_\infty^3}{3k * k_\infty}, Q = \frac{Q_0(T_W - T_\infty)}{c_p C_p(T_f - T_\infty)}, Re = \frac{U_s x}{v_\infty}, \beta = \frac{C_f - C_\infty}{C_\infty}$

$$Ec = \frac{U_W^2}{C_p(T_W - T_\infty)}, Sc = \frac{v_\infty}{D_B}, \gamma_1 = \frac{k_2^2}{b}, E = \frac{E_e}{\lambda T_\infty}, \zeta = \frac{h_f}{k_\infty}\sqrt{\frac{v_\infty}{b}}, We = \Gamma\sqrt{2\frac{c^3 x^{3r-1}}{v_\infty}} \quad (11)$$

$Nb = \frac{(\rho c_p)_p D_B(G_W - G_\infty)}{(\rho c_p)f v}, Nt = \frac{(\rho c_p)_p D_T(T_W - T_\infty)}{(\rho c_p)_f T_\infty v}, \gamma = \frac{(\rho c)_p}{(\rho c)_f}, H = \frac{c}{b}$

The developing physical terms listed in equation (11) are: E_c denotes Eckert number, N_r indicates radiation term, E_e indicates Weissenberg number while K defines the stretching ratio, γ_1 denotes the chemical reaction term, ϵ shows the thermal conductivity term, E symbolizes the activation energy, β is the temperature relative parameter, M shows the magnetic, δ is the concentration relative parameter, N_t is the thermo-migration term while N_b describes the haphazard motion of the minute particles, whereas $Sc(Pr)$ defines the Schmidt Prandtl number. For the engineering implementation of the current study, those quantities of interest are outlined as (i) the skin drag coefficient C_{fx} (ii) the Nusselt number Nu_x and (iii) the Sherwood number Sh_x are respectively expressed as,

$$C_{fx} = \frac{2\tau_w}{\rho_\infty U_8^2}, Nu_x = \frac{xq_w}{k_\infty(T_f - T_\infty)}, Sh_x = \frac{xq_m}{D_B(C_W - C_\infty)} \quad (12)$$

The dimensionless forms of the quantities in equation (12) are expressed as:

$$C_{fx}^* = \frac{1}{2} Re^{\frac{1}{2}} C_{fx} = \left(f''(0) + \frac{We}{2} f''^2(0)\right), \quad (13)$$

We also note that,

$Nu_x^* = Re_x^{-\frac{1}{2}} Nu_x = -(1 + nr)\theta'(0), Sh_x^* = Re_x^{-\frac{1}{2}} Sh_x = -\phi'(0).$

where

$$\tau_w = \mu_\infty\left[\frac{\partial u}{\partial y} + \frac{\Gamma}{\sqrt{2}}\left(\frac{\partial u}{\partial y}\right)^2\right]_{y=0}, \; q_w = -\left[\left(k_\infty + \frac{16T^3\sigma^*}{3k^*}\right)\frac{\partial T}{\partial y}\right]_{y=0}, \; q_m = -\left(D_B\frac{\partial C}{\partial y}\right)_{y=0} \quad (14)$$

Numerical Method with Validation

For the system of equations (7-9) and its wall constraints expressed in equation (10), we have employed a numerical means to obtain the required solution because the set of equations (7-9) has a grater dimension of nonlinearity nature. The Runge-Kutta-Gills techniques has been applied having step size $\nabla_\eta = 0.01$ with absolute tolerance of 10^5. The program had been implemented on Maple 16. The results have been authenticated by comparing the computational data of f″(0) for alterations in M with some existing results under restrictive conditions as displayed in Table 2. There are good agreement in the current work and those already reported in (Mabood et. al., 2021).

Table 1: Computed data for f″(0) for variation in M

M	Mabood et al., (2021)	Present results
0	1.000005	1.00000
1	-1.4142143	-1.41421
5	-2.4494893	-2.44949
10	-3.3166242	-3.31662
50	-7.1414285	-7.14143
100	-10.049876	-10.0499

Outcomes of the analysis and deliberation

Further to the discussions so far, some new results showing the impact of various developing terms on the profiles of the dimensionless quality of interest have been obtained. Thus, the effects of some important parameters as it affects the velocity field and temperature region have been considered and the emerging results displayed in Figure 2 and Figure 3. Figure 2 has shown the behaviour of the magnetic field element M as it affects the trend of the velocity. As M increases, flow is stifled because the transverse magnetic field exerts a Lorentz force on the electrically conducting Williamson fluid causing resistance to its motion. The flow of the fluid is slowed because when M increases, the Lorentz force also increases, and vice versa. In view of this, there is a thinning of the hydrodynamic bounding structure.

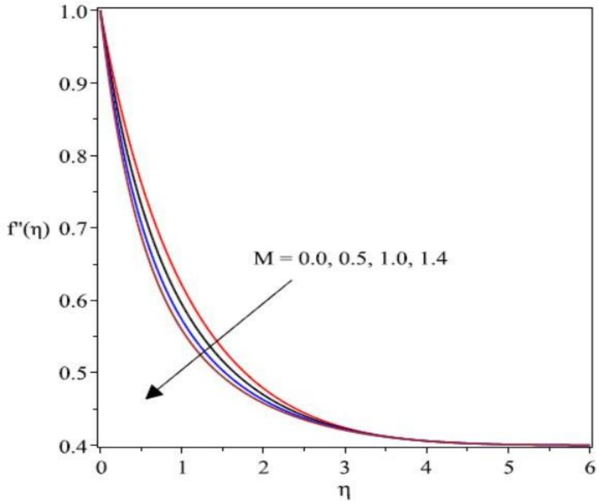

Figure 2: Velocity field profile due to variation in M

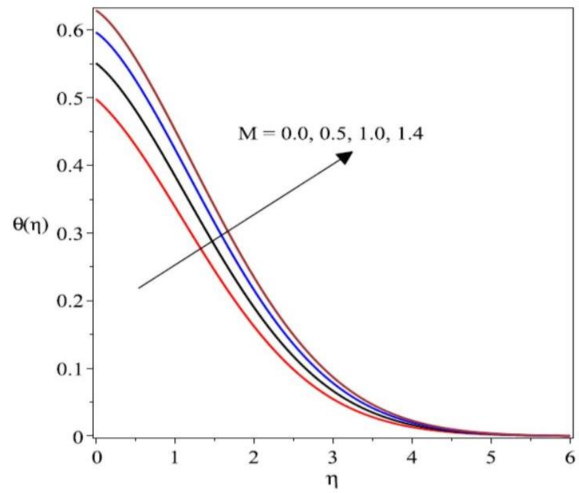

Figure 3: Trend in temperature profile due to variation in M

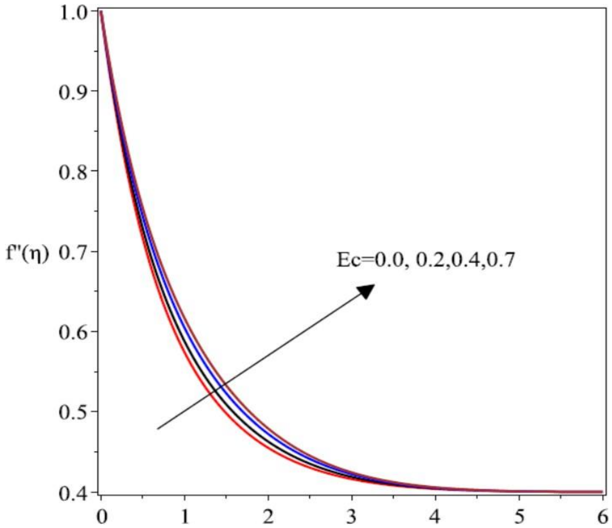

Figure 4: Trend of velocity field as Ec alters

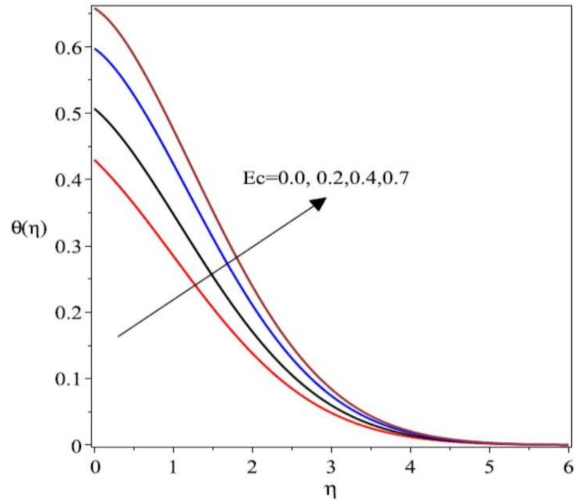

Figure 5: Trend in temperature profile due to variation in Ec

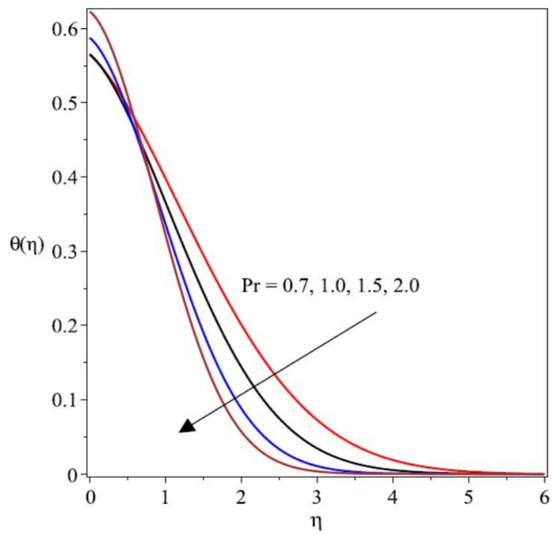

Figure 6: Trend of temperature due to variation in Pr.

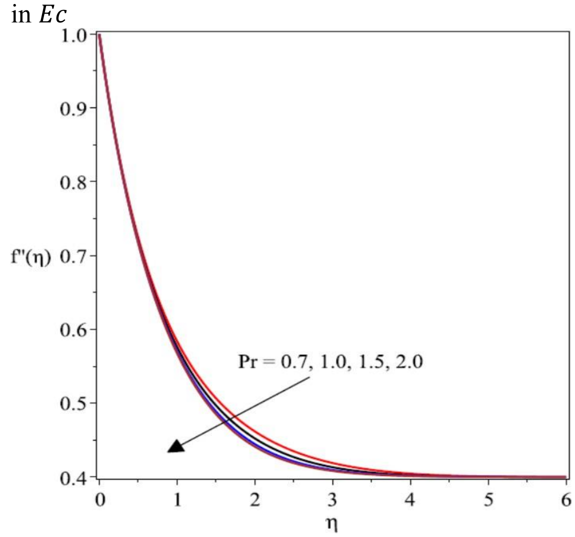

Figure 7: Plot of the velocity field due to variation in Pr

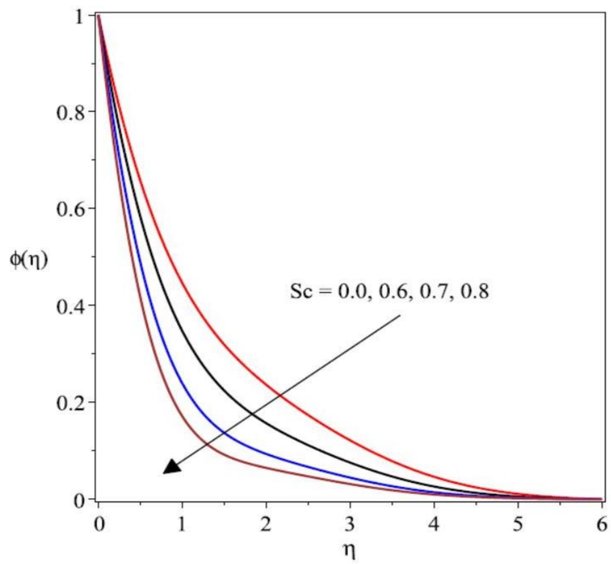

Figure 8: Trend of the concentration profiles due to variation in Sc

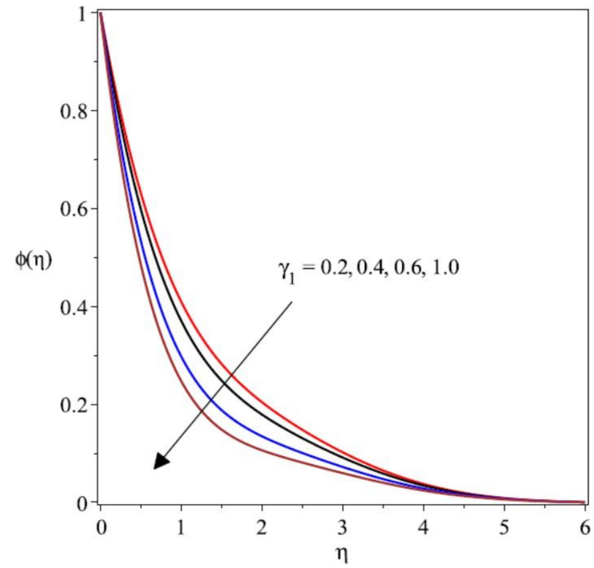

Figure 9: Behaviour of concentration due to variation in γ1

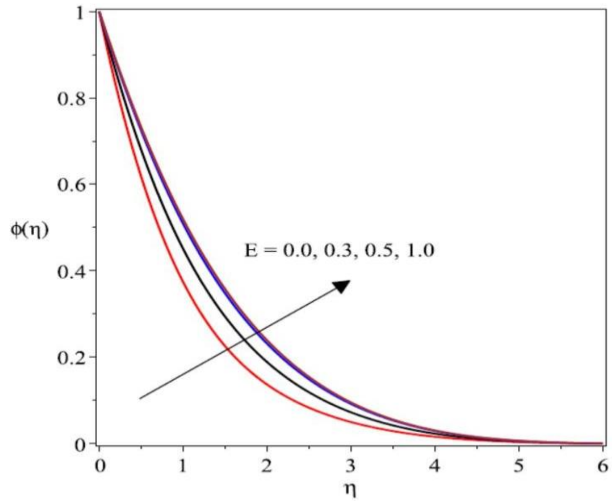

Figure 10: Trend of the concentration due to varying E9

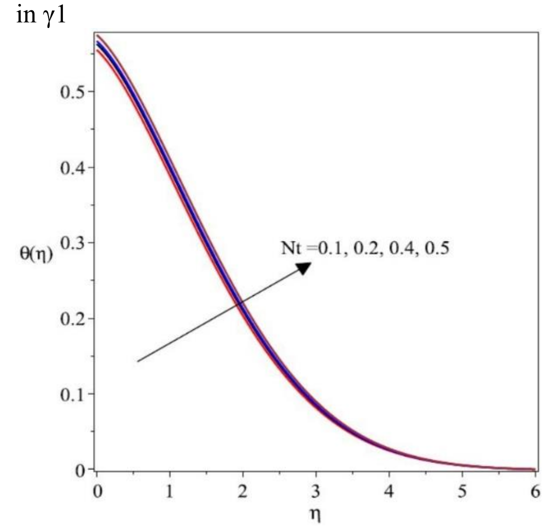

Figure. 11: Trend of the temperature due to varying Nt

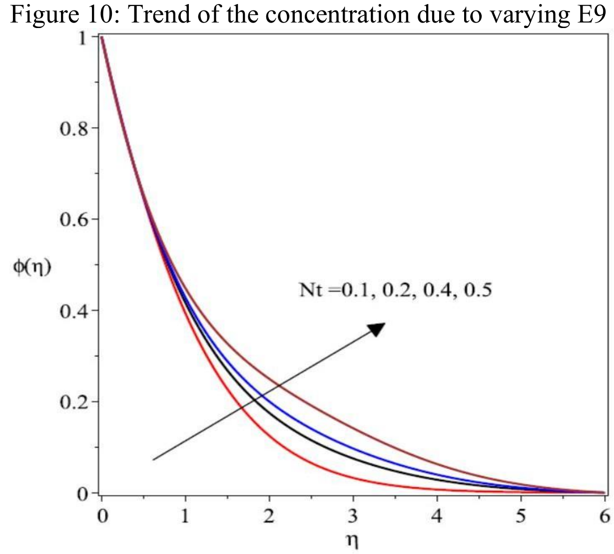

Figure. 12: Trend of the concentration due to varying Nt

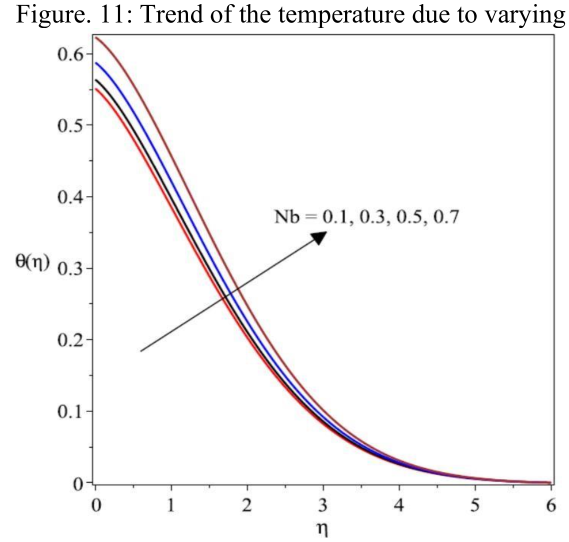

Figure. 13: Trend of the concentration due to varying Nb

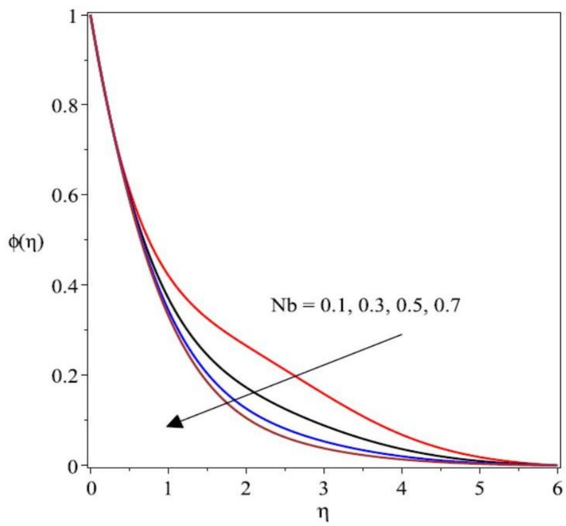

Figure. 14 Trend of the concentration due to variation in Nb values

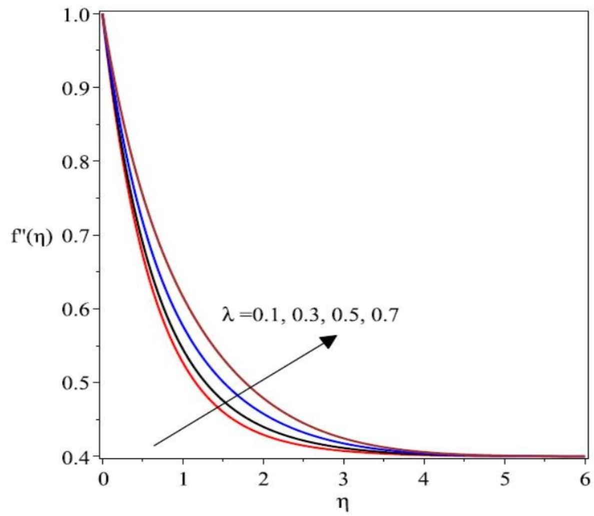

Figure. 15 Trend of the velocity due to variation in the value of λ.

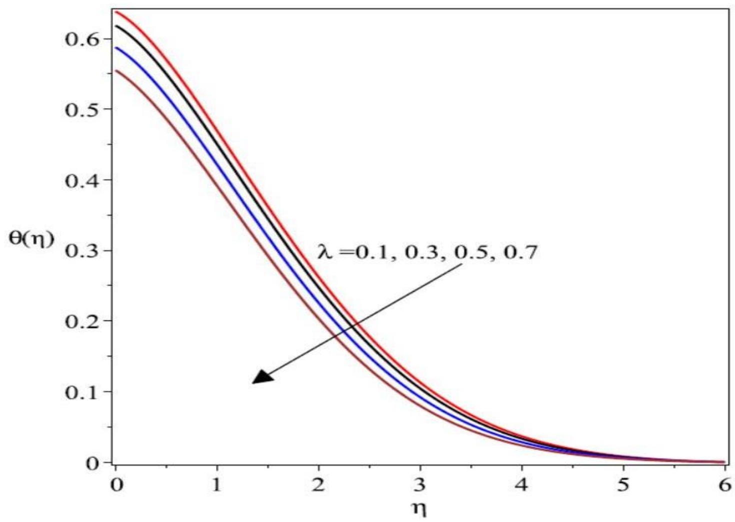

Figure. 16 Trend of the temperature as a result of variations in λ

RESULTS AND DISCUSSION

In Figure 3, temperature field becomes energized due to friction as a result of growth in M. Here, the interaction of the Lorentz force and the electric nature of the Williamson fluid prevents the mobility of the fluid due to a magnetic field M Consequently, there is an upsurge in resistance, which in effect, enables a rise in the heat profiles. This incident causes increase in temperature, and the thermal boundary structure increases considerably as the magnitudes of M increases. Hence, the flow and thermal distribution can be adjusted fittingly by the modifications of the magnetic field term in the fluid zone.

Transport phenomena for the heat and motion profiles due to variation in the Ec values are displayed in Figures 4 and 5. Increasing Ec values caused an upward shift in the velocity profiles. The thermal neighborhood also increases in value dramatically with increasing Ec. As Ec increases, more heat is generated in the flow field because of the frictional impact of the Williamson fluid particles and the growing sheet. In fact the thermal bounding surface is seen to enlarge noticeably with increasing Ec.The behavioural pattern of the velocity field and that of the thermal region are displayed in Figures 6 and 7 due to variation in P_r. Pr describes the viscousness of the momentum layer compared to that of the thermal zone.

Figure 6 indicates that the velocity profiles falls due to variation in Pr because there is a direct relationship between Pr and Williamson fluid viscosity, and so growth in Pr corresponds to higher viscosity, and thereby creates resistance to the fluid speed. At the same time, the thermal bounding structure thins out as Pr magnifies. As a result, there is a cooling effect as the surface temperature falls significantly.

The concentration of nanoparticles is shown to decline in nature as Sc improves in magnitude, as depicted in figure 8. It is known that Sc is a description of the thickness of the momentum layer compared to that of the concentration layer. In this plot, a rise in Sc causes the mass diffusivity to drop. Hence, there is a reduction in the concentration bounding surface. Meanwhile, figure 9 depicts the trend of the concentration profiles versus η as the chemical reaction term changes in value. The concentration of the tiny particles is a decreasing function of γ1, as found in figure 9. A rise in activation energy parameter

boosts the growth of the concentration profiles, as exemplified in figure 10. As is known, E describes the minimum amount of energy required for a reaction process to begin. So, an increase in E energizes the reaction to take place in the concentration region, which led to the expansion of the profiles as portrayed in this figure.
The illustration of the thermal and solutal fields due to the alteration in the in Nt is sketched in figures 11 and 12. Clearly, both profiles upsurge due to rising values of Nt. Also, the temperature field field enhances due to the irregular movement of the minute particles Nb as found in Figure 13.
However, the concentration field reacts in a diametric manner as it falls significantly in the face of Nb as clearly seen in Figure 14. Figure 14 demonstrates that N_b produces a thin layer in the boundary structure and as such causes a decline in the concentration profiles.
Figure 15 and 16 shows the behaviour of the mixed convection term on the velocity and thermal profiles. A boost in λ causes the upthrust to appreciate over that of drag force and thus, the velocity profiles improves, leading to higher fluid flow motion as found in Figure 15. On the other hand, Figure 16 shows the plot where thermal bounding surface declines due to growing values of the mixed convection term.

CONCLUSION

This study examines the stream of hydromagnetic Williamson nanofluids over a nonlinear stretchable sheet in a material device experiencing non-uniform thermal conductivity. In the heat wall region where convective heat restrictions are present, the effects of viscous dissipation, buoyancy force, mixed convection, thermal radiation, activation energy, and chemical processes have been examined. The relevant governing partial differential equations have been analysed and transformed to ordinary differential equations of order three using a similarity modification method. Furthe simplification was achieved using the Runge-Kutta Fehlberg approach with the shooting method. Findings are displayed in tables and plots for the ease of interpretation. The findings were found to be in good agreement with the existing results. A few key takeaways from this study are the Lorentz force applies a transverse magnetic field to an expanding plate causes the Williamson fluid to experience a significant slowing of its velocity, the effects of the Prandtl number dampen the fluid's motion, whereas the Eckert number and mixed convection characteristics cause the movement of fluid to surge, thermo-migration of small particles and erratic behavior of minute particles in the thermal region, was found to enhance heat dispersion as the Eckert number increases the temperature of the fluid, the effects of variation of Sc and γ1 caused the concentration profiles to decrease with the activation energy (E) producing a considerable upward shift in the concentration profiles.

REFERENCES

Chao, B. T., & Jeng, D. R. (1965). Unsteady stagnation point heat transfer. *Journal of Heat Transfer,* 87, 221–230.

Choi, S. U. S. (1995). Enhancing thermal conductivity of fluids with nanoparticles. *International Mechanical Engineering Congress and Exposition,* 66, 99–105.

Cortell, R. (2007). Viscous flow and heat transfer over a nonlinearly stretching sheet. *Applied Mathematics and Computation,* 184, 864–873.

Crane, L. J. (1970). Flow past a stretching plate. *Communications Breves, 21*, 645–647.

Fatunmbi, E. O., Ogunseye, H. A., & Sibanda, P. (2020). Magnetohydrodynamic micropolar fluid flow in a porous medium with multiple slip conditions. *International Communications in Heat and Mass Transfer,* 115, 104577. https://doi.org/10.1016/j.icheatmasstransfer.2020.104577

Fatunmbi, E. O., Ramonu, O. J., & Salawu, S. O. (2023). Analysis of heat transfer phenomenon in hydromagnetic micropolar nanoliquid over a vertical stretching material featuring convective and isothermal heating conditions. *Waves in Random and Complex Media.* https://doi.org/10.1080/17455030.2023.2173494

Gupta, P. S., & Gupta, A. S. (1977). Heat and mass transfer on a stretching sheet with suction or blowing. *Canadian Journal of Chemical Engineering, 55*, 744–746.

Ibrahim, S. M., & Suneetha. (2015). Effects of heat generation and thermal radiation on steady MHD flow near a stagnation point on a linear stretching sheet in porous medium. *Journal of Computational and Applied Research in Mechanical Engineering*, 4, 133–144.

Mahanthesh, B., Mackolil, J., Radhika, M., Al-Kouz, W., & Siddabasappa. (2020). Significance of quadratic thermal radiation and quadratic convection on boundary layer two-phase flow of a dusty nanoliquid past a vertical plate. *International Communications in Heat and Mass Transfer.* https://doi.org/10.1016/j.icheatmasstransfer.2020.105029

Mabood, F., Khan, W. A., & Ismail, A. I. M. (2015). Approximate analytical modeling of heat and mass transfer in hydromagnetic flow over a non-isothermal stretched surface with heat generation/absorption and transpiration. *Journal of the Taiwan Institute of Chemical Engineers,* 54, 11–19.

Mabood, F., Yusuf, T. A., & Khan, W. A. (2021). $CuAl_2O_3$-H_2O hybrid nanofluid flow with melting heat transfer, irreversibility analysis, and nonlinear thermal radiation. *Journal of Thermal Analysis and Calorimetry,* 143(2), 973–984.

Mishra, S. R., Baag, S., & Mohapatra, D. K. (2016). Chemical reaction and Soret effects on hydromagnetic micropolar fluid along a stretching sheet. *Engineering Science and Technology, an International Journal,* 19, 1919–1928.

Nabwey, H. A., & Mahdy, A. (2021). Transient flow of micropolar dusty hybrid nanofluid loaded with Fe_3O_4-Ag nanoparticles through a porous stretching sheet. *Results in Physics,* 21, 103777.

Nadeem, S., Hussain, S. T., & Lee, C. (2013). Flow of a Williamson fluid over a stretching sheet. *Brazilian Journal of Chemical Engineering,* 30(3), 615–625.

Pal, D., & Chatterjee, S. (n.d.). Heat and mass transfer in MHD non-Darcian flow of a micropolar fluid over a stretching sheet embedded in a porous media with non-uniform heat source and thermal radiation.

Pandey, A. K., & Kumar, M. (2016). Effect of viscous dissipation and suction/injection on MHD nanofluid flow over a wedge with porous medium and slip. *Alexandria Engineering Journal,* 55(4), 3115–3123.

Qasim, M., Khan, I., & Shafie, S. (2013). Heat transfer in a micropolar fluid over a stretching sheet with Newtonian heating. *PLoS ONE,* 8(4), 1–6.

Quran, O., Maaitah, H., & Duwairi, H. M. (2023). Fluid flow and heat transfer characteristics of Williamson fluids flowing in saturated porous media. *Advances in Mechanical Engineering.* https://doi.org/10.1177/16878132231115715

Sajjan, K., Shah, N. A., Ahammad, N. A., Raju, C. S. K., Kumar, M. N., & Weera, W. (2022). Nonlinear Boussinesq and Rosseland approximations on 3D flow in an interruption of ternary nanoparticles with various shapes of densities and conductivity properties. *AIMS Mathematics,* 7(10), 18416–18449. https://doi.org/10.3934/math.20221014

Shah, Z., Bonyah, E., Islam, S., Khan, W., & Ishaq, M. (2018). Radiative MHD thin film flow of Williamson fluid over an unsteady permeable stretching sheet. *Heliyon,* 4, e00825. https://doi.org/10.1016/j.heliyon.2018.e00825

Wang, C. Y. (1984). The three-dimensional flow due to a stretching flat surface. *Physics of Fluids,* 27, 1915. https://doi.org/10.1063/1.864868

Waqas, M., Farooq, M., & Khan, M. J. (2016). Magnetohydrodynamic (MHD) mixed convection flow of micropolar liquid due to nonlinear stretched sheet with convective condition. *International Journal of Heat and Mass Transfer,* 102, 766–772.

Williamson, R. V. (1929). The flow of pseudoplastic materials. *Industrial and Engineering Chemistry,* 21(11), 1108–1111.

Yusuf, S.I., Ejeh S. and Olayiwola, R.O. (2021). Analysis of Leakages of Non-Viscous Flow in a Pipe Using Mass Flow Rate. *Nigeria Journal of Physics,* 30(2), 51-57.